PZR coordinates Noonan and LEOPARD syndrome signaling in zebrafish and mice

Jeroen Paardekooper Overman[1,#], Jae-Sung Yi[2,#], Monica Bonetti[1], Matthew Soulsby[2], Christian Preisinger[3,4], Matthew P. Stokes[5], Li Hui[5], Jeffrey C. Silva[5], John Overvoorde[1], Piero Giansanti[3], Albert J.R. Heck[3], Maria I. Kontaridis[6], Jeroen den Hertog[1,7,*] and Anton M. Bennett[2,8,*]

1. Hubrecht Institute-KNAW and University Medical Center Utrecht, Utrecht, Netherlands 2. Department of Pharmacology, Yale University School of Medicine, New Haven, Connecticut 06520, USA 3. Department of Biomolecular Mass Spectrometry and Proteomics, Utrecht, The Netherlands 4. Current address: Proteomics Facility, Interdisciplinary Centre for Clinical Research (IZKF) Aachen, Pauwelsstraße 30, Aachen Germany 52074 5. Cell Signaling Technology, Danvers, MA 01923, USA 6. Harvard Medical School, Department of Cardiology, Beth Israel Deaconess Medical Center, 3 Blackfan Circle, Boston, MA 02115 7. Institute Biology Leiden, Leiden, Netherlands 8. Program in Integrative Cell Signaling and Neurobiology of Metabolism, Yale University School of Medicine, New Haven, Connecticut 06520, USA #; Equal contributing authors. *These authors directed jointly the work

Molecular and Cellular Biology, 2014, August 34(15): 2874-2889

Abstract

Noonan syndrome (NS) is an autosomal dominant disorder caused by activating mutations in the *PTPN11* gene encoding for Shp2, which manifests in congenital heart disease, short stature and facial dysmorphia. The complexity of Shp2 signaling is exemplified by the observation that LEOPARD syndrome (LS) patients possess inactivating *PTPN11* mutations yet exhibit similar symptoms to NS. Here, we identify protein zero-related (PZR), a transmembrane glycoprotein, which interfaces with the extracellular matrix to promote cell migration, as a major hypertyrosyl phosphorylated protein in mouse and zebrafish models of NS and LS. PZR hypertyrosyl phosphorylation is facilitated in a phosphatase-independent manner by enhanced Src recruitment to NS and LS Shp2. In zebrafish, PZR overexpression recapitulated NS and LS phenotypes. PZR was required for zebrafish gastrulation in a manner dependent upon PZR tyrosyl phosphorylation. Hence, we identify PZR as a NS and LS target. Enhanced PZR-mediated membrane recruitment of Shp2 serves as a common mechanism to direct overlapping pathophysiological characteristics of these *PTPN11* mutations.

Introduction

The Src homology 2 (SH2) domain-containing protein tyrosine phosphatase-2 (Shp2) is an ubiquitously expressed non-transmembrane protein tyrosine phosphatase (PTP) encoded by the *PTPN11* gene [1]. Shp2 comprises of two SH2 domains, a PTP domain and a C-terminal tail that contains a proline rich region flanked by two tyrosine phosphorylation sites. The SH2 domains of Shp2 serve to direct protein-protein interactions with its upstream phosphotyrosyl target in a sequence-specific context and the SH2 domains participate in maintaining a closed conformation by establishing contacts with the PTP domain [2]. The phosphatase domain of Shp2 catalyzes substrate-specific dephosphorylation and is tightly regulated. In the basal state, the catalytic activity of Shp2 is suppressed by Shp2 assuming a "closed" conformation maintained through the NH2-terminal SH2 (N-SH2) domain forming surface contacts with the PTP domain, which occludes the catalytic site. SH2 domain engagement disrupts this "closed" conformation leading to allosteric modulation and exposure of the catalytic site in to an "open" state that is now substrate accessible [2]. Engagement of the SH2 domains provides an elegant molecular switch mechanism to activate the phosphatase that allows for targeted substrate dephosphorylation within a precise micro-environment. As such, the repertoire of Shp2-binding proteins plays a major role in dictating Shp2 signaling complexity and specificity. Consistent with this, interference of Shp2's SH2 domains abrogates both physiological and pathophysiological signaling [3]. Thus, the integrity of the SH2 domains of Shp2 plays a critical role in its ability to signal.

A wealth of biochemical, cellular and genetic evidence in mice, *Drosophila* and zebrafish has established that Shp2 plays a positive signaling role downstream of numerous receptor tyrosine kinases, cytokine receptors, G protein-coupled receptor and integrins [1]. The repertoire of Shp2-interacting proteins in combination with a wide variety of substrates [4] endows this phosphatase the capability of engaging a complex array of signaling molecules and pathways such as the Ras/MAPK, PI3K/Akt, JAK/STAT, RhoA/Rac and Src family kinases (SFKs). Shp2 has been shown to promote a number of cellular functions including cell growth, cell survival and differentiation, hence affecting organismal functions such as development in mice [5,6], *Drosophila* [7] and zebrafish [8]. The highly conserved nature of Shp2 signaling in lower organisms has provided powerful model systems for the genetic dissection of Shp2 function in development. The realization that Shp2 plays an important role in human development arose through the discovery that germline mutations in the *PTPN11* gene encoding for Shp2 cause two similar types of autosomal dominant disorders [9,10]. More than 50% of Noonan syndrome (NS) (NIM163950) cases are caused by mutations in *PTPN11* that result in increased Shp2 catalysis. In contrast, as much as 90% of LEOPARD syndrome (LS) (NIM151100) mutations are caused by inactivating *PTPN11* mutations that gives rise to impaired Shp2 activity.

NS and LS are autosomal dominant disorders that manifest in short stature, ocular hypertelorism, cardiac defects, webbed neck and increased incidence of mental retardation [11-13]. NS and LS comprise part of a larger series of disorders that have thus far been characterized by mutations in components of the Ras/MAPK pathway and are collectively referred to as "RASopathies" [14]. As such, NS and LS exhibit overlapping clinical presentations such as proportionate short stature, facial dysmorphia, musculoskeletal anomalies and to a lesser extent congenital heart disease. Despite the similarities between NS and LS, these "RASopathies" are caused by opposite effects on Shp2 activity [9,15-18]. These observations suggest that NS and LS may utilize common signaling components in the pathogenesis of these developmental disorders. Interestingly, one common feature of both NS and LS mutants is that both forms of Shp2 exhibit an increased

propensity to adopt an "open" conformation, leading to increased affinity to upstream target binding through the SH2 domains and target substrates [2,8,19,20]. Hence, the "open" conformation of NS and LS disease mutants may underlie the molecular pathogenesis of these syndromes rather than altered substrate dephosphorylation by the PTP domain. Despite these highly plausible explanations it remains unclear how activating and inactivating mutants of Shp2 liberate overlapping disease outcomes. Moreover, identification of the target(s) for both NS and LS that must presumably be shared in order for them to elicit overlapping clinical outcomes is unknown.

PZR is a transmembrane glycoprotein with an extracellular immunoglobulin (Ig) domain and an intracellular domain containing two immunoreceptor tyrosine-based inhibitory motifs (ITIMs) [21-23]. The ITIMs, when tyrosyl phosphorylated, serve as Shp2 binding sites [21]. We had identified previously that NS-associated Shp2 mutants induce PZR hypertyrosyl phosphorylation and recruit increased Shp2. Moreover, in *Ptpn11*$^{D61G/+}$ mouse embryos PZR is hypertyrosyl phosphorylated demonstrating that it is aberrantly regulated in NS mice during development. Interestingly, PZR is upregulated during blastocyst formation [24]. Moreover, in mouse embryo fibroblasts derived from NS mice, adhesion-dependent ERK1/2 activation is abrogated upon loss of PZR expression [25].

To gain further insight in to how NS and LS might liberate similar phenotypes we performed an unbiased phosphotyrosine proteomics screen in a mouse model of NS and a zebrafish model of NS and LS. We identified protein zero-related (PZR) as a major hypertyrosyl phosphorylated protein in both NS and LS in mice and zebrafish. The role of PZR in development remains unclear and the pathophysiological significance of PZR/Shp2 interactions in NS and LS is also unknown. NS and LS are linked to defects in gastrulation cell movements and Shp2 is essential for gastrulation movements in mouse and zebrafish [11,26]. We show that PZR/Shp2 interactions are required for gastrulation in zebrafish. These results define a functional role for PZR in an intact organism. Moreover, they suggest that PZR is a common target that contributes to altered development in cases of both NS and LS.

Results

PZR is a major hypertyrosyl phosphorylated protein in NS.

Since NS and LS exhibit overlapping clinical outcomes we set out to identify target proteins that are affected by both syndromes. We hypothesized that targets similarly altered in their levels of tyrosyl phosphorylation in both NS and LS likely represent molecules of convergence in these diseases. Given that NS and LS mutants exhibit opposite catalytic activities we reasoned that a phosphatase-independent mechanism likely represents a common pathway for these two syndromes. Therefore, we focused on the identification of hypertyrosyl phosphorylated proteins in a mouse model of NS rather than hypotyrosyl phosphorylated ones, since the latter likely represents phosphatase-dependent Shp2 substrates.

We performed a phosphotyrosyl proteomics screen in mice harboring a knock-in of a NS-associated Shp2 mutant [27]. Mice containing an Asp61 to Gly61 (D61G) mutation within the NH2-terminal SH2 domain of Shp2 (Shp2^{D61G}) generates a NS mutation found in humans [9]. Heterozygous progeny of these mice (*Ptpn11*$^{D61G/+}$) recapitulate several NS features observed in humans such as cardiovascular and skeletal abnormalities [27]. Since both NS and LS exhibit

significant clinical defects in the heart we focused on this tissue. We performed a global survey of the levels of tyrosyl phosphorylated proteins in the hearts of 5 day-old wild type and *Ptpn11*$^{D61G/+}$ mice using an immunoaffinity phosphoproteomics approach [28]. The relative abundance of tyrosyl phosphorylated proteins was assessed by quantitating the frequency of phosphopeptides derived from wild type and *Ptpn11*$^{D61G/+}$ mice [28]. We identified an approximately equal

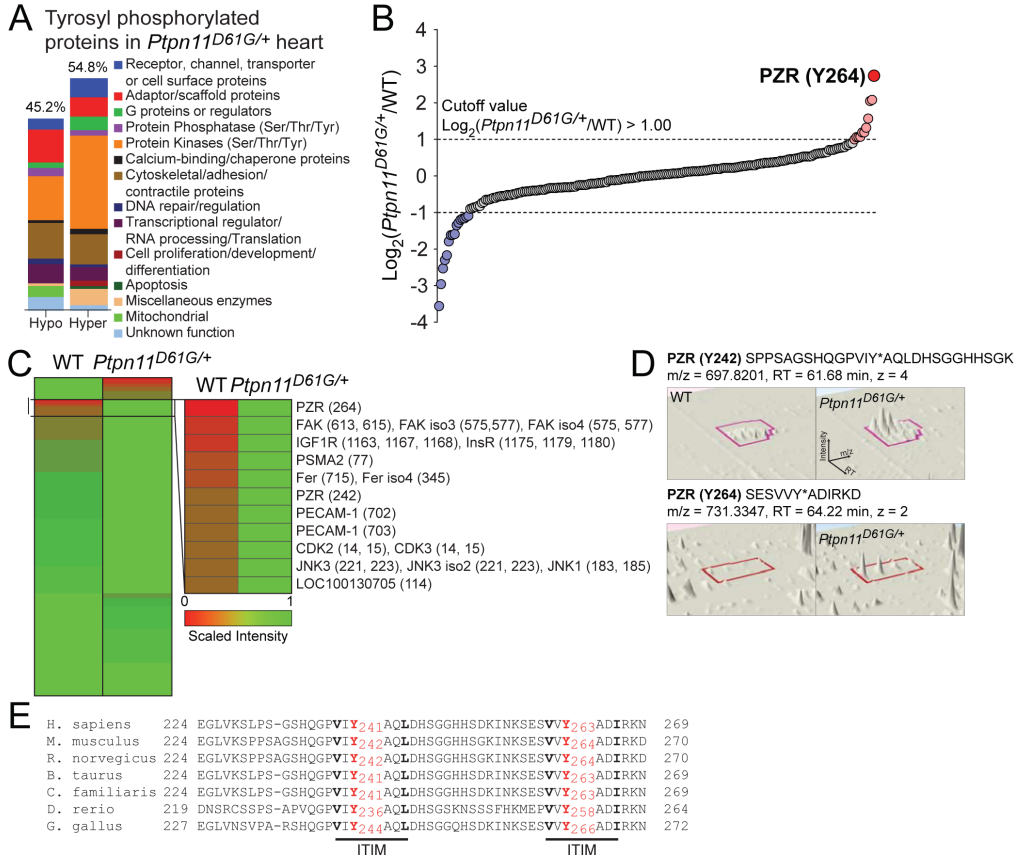

Figure 1 Proteomic analysis of differentially tyrosyl phosphorylated proteins in hearts of *Ptpn11*$^{D61G/+}$ mice. (A) Classification of hypo and hyper-tyrosyl phosphorylated proteins in the hearts of *Ptpn11*$^{D61G/+}$ mice. (B) Log_2-transformed values for the ratio of each phosphotyrosine-containing peptide in wild type and *Ptpn11*$^{D61G/+}$ mouse hearts. (C) Heat map of differentially tyrosyl phosphorylated peptides. (D) Extracted ion chromatogram and peptide sequence of PZR-containing tyrosine 242 (upper panels) and tyrosine 264 (lower panels) by differential proteomics. (E) Amino acid sequences of PZR C-terminus in different vertebrates. Consensus sequences for ITIM (S/I/V/LxYxxI/V/L) are indicated in bold and tyrosine residues are marked red with their appropriate amino acid numbering.

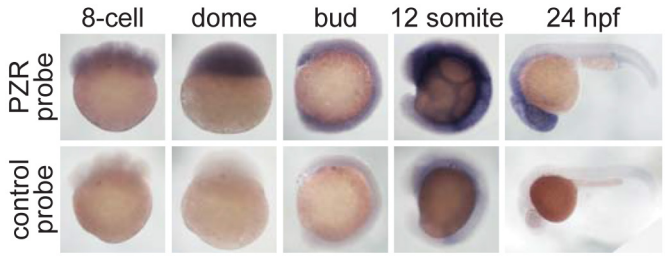

Figure 2 Expression pattern of PZR in developing zebrafish. *In situ* hybridization for PZR was performed on developing zebrafish embryos at 8-cell, dome, bud, 12-somite stage and at 24 hpf. The PZR sense probe was used as a control

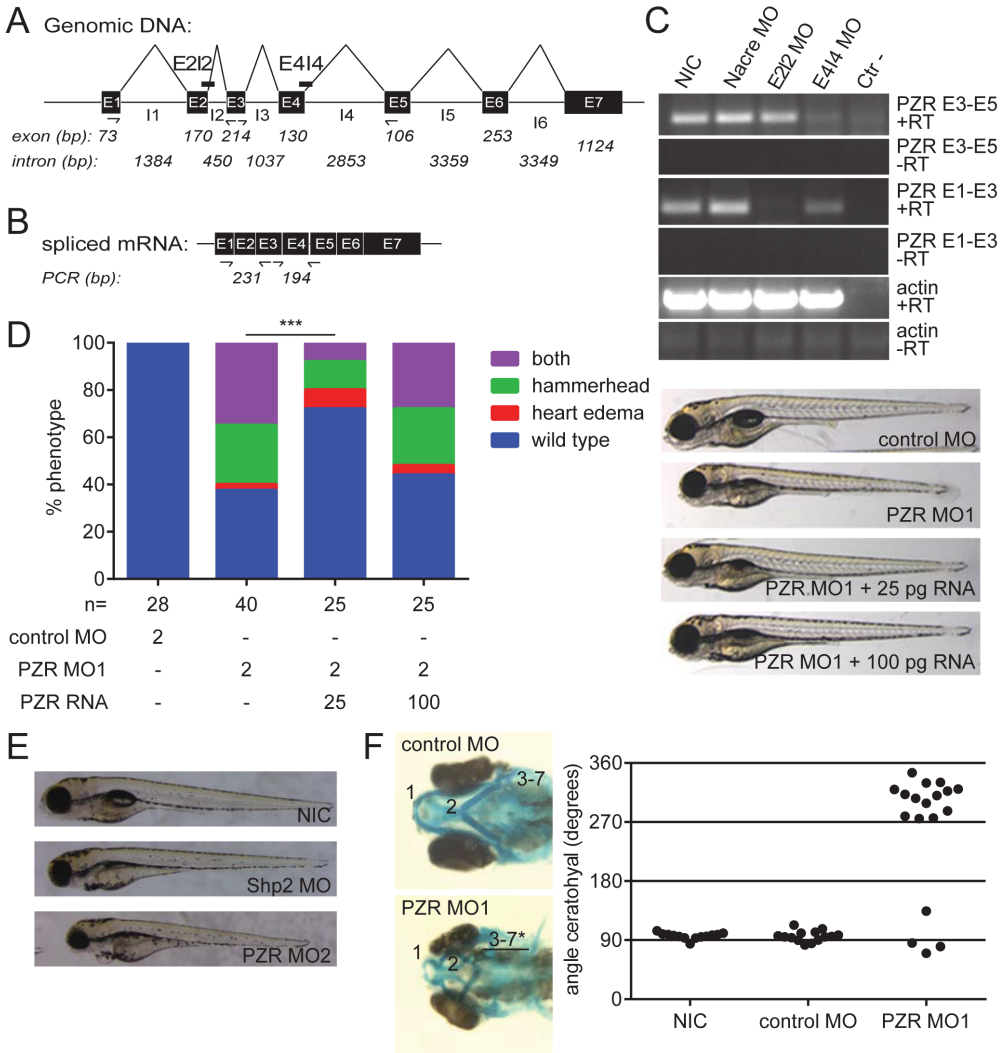

Figure 3 PZR is required for zebrafish development. (A) Genomic organization of zebrafish *mpzl1* gene encoding PZR. The target sites of E4I4MO (PZR-MO1) and E2I2 MO (PZR-MO2) are indicated as well as the positions of the oligonucleotides used for amplification of E3/E5 and E1/E3. (B) PZR mRNA and the positions of the oligos used for RT-PCR are depicted; the size of the PCR products is shown (bp). (C) Embryos were untreated (non-injected control, NIC) or injected at the one-cell stage with control MO (Nacre MO), PZR E2I2MO (PZR-MO2) or E4I4 MO (PZR MO1). PCR was performed for E3/E5, or E1/E3. (ctr-) indicates water control. (D) Embryos were injected (1-cell stage) with 2 pg control MO, 2 pg PZR MO or co-injected with 25 pg or 100 pg PZR mRNA. Embryos were scored at 4 dpf. (E) Zebrafish embryos were injected at the 1-cell stage with 2 ng Shp2 MO or 2 ng PZR MO2 or 2 ng control morpholino and photographed at 3 dpf. (F) Embryos were injected at the 1-cell stage with 2 pg PZR MO, 2 pg control MO or non-injected as a control, fixed at 4 dpf and stained with alcian blue. Meckel's cartilage (1), the ceratohyal (2) and branchial arches (3-7) are indicated. The angle of the ceratohyal was measured.

repertoire of differentially hypo and hypertyrosyl phosphorylated peptides in the hearts of *Ptpn11*$^{D61G/+}$ mice (Figure 1A and B). The limited number of differentially tyrosyl phosphorylated peptides suggests that the NS mutant induces a discrete influence on global tyrosyl phosphorylation levels in the heart (Figure 1B). The highest induced hypertyrosyl phosphorylated peptide represented Y264, which is present in the transmembrane glycoprotein, protein zero-related (PZR) and was induced by 6.7-fold as compared to wild type controls (Figure 1C and D). The sequence surrounding Y264 was identified to be part of the immunoreceptor tyrosine inhibitory motif (ITIMs) of PZR [23]. PZR contains two ITIMs both of which are highly conserved among vertebrates and when phosphorylated binds directly to the SH2 domains of Shp2 [23]. Notably, the other tyrosine-containing ITIM on PZR represented by Y242 was also detected to be hypertyrosyl phosphorylated by 2.2-fold (Figure 1C and D). For clarity, we will use the human amino acid numbering of PZR (Figure 1E - mouse Y242 and Y264 correspond to human Y241 and Y263, respectively). Previously, we found that PZR was hypertyrosyl phosphorylated during embryogenesis in *Ptpn11*$^{D61G/+}$ mice [25]. These results identify Y242 and Y264 as sites of PZR hypertyrosyl phosphorylation in this mouse model of NS.

Zebrafish have been shown to recapitulate both NS and LS phenotypes [11]. Therefore, phosphotyrosyl proteomics screens were performed in developing (26 hours post-fertilization) embryos to identify differentially tyrosyl phosphorylated peptides between zebrafish embryos expressing either NS or LS mutants as compared with controls. When injected with the Shp2^{D61G} NS mutant, peptides representing the ITIMs of zebrafish PZR containing Y241 and Y263 were identified to be amongst the highest induced phosphotyrosyl-containing peptides (7.7 and 4.7-fold increase for Y241 and Y263, respectively as compared with controls). In addition, LS-injected embryos also were found to contain PZR hypertyrosyl phosphorylated peptides at both Y241 and Y263 representing increases of 3.4- and 3.1-fold relative to wild type controls. These results identify PZR as a major hypertyrosyl phosphorylated target in zebrafish embryos expressing either NS or LS mutations.

PZR is expressed ubiquitously and functions in the Shp2 pathway in zebrafish.

Our data demonstrate that PZR tyrosyl phosphorylation is aberrantly regulated in NS mouse embryos and post-developmentally in NS hearts ([25] and Figure 1) and during development of NS/LS expressing zebrafish embryos. These results suggest that altered PZR tyrosyl phosphorylation may play a role in NS and LS pathogenesis. To further examine the role of PZR during zebrafish development we determined the expression of *mpzl1*, the gene encoding zebrafish PZR. Zebrafish PZR was cloned and was used to generate an *mpzl1*-specific probe. *In situ* hybridization of *mpzl1* expression was apparent from the 8-cell stage onwards, indicating maternal expression. *Mpzl1* expression was ubiquitous until bud stage and at later stages *mpzl1* expression appeared to be enhanced anteriorly (Figure 2). The specificity of the antisense *mpzl1* probe was confirmed by the lack of signal of the sense control probe in parallel experiments (Figure 2). Thus, PZR is maternally contributed and expressed at embryonic stages during and after zebrafish gastrulation.

PZR knockdown phenocopies NS and LS expression in zebrafish embryos.

Next, PZR was knocked down in order to investigate the role of PZR in zebrafish signaling. The specificity of the PZR MO to block PZR splicing was confirmed (Figure 3A - C). Knockdown of PZR, but not a control morpholino (MO), induced a phenotype characterized by reduced body axis length (4.9 ± 1.1 % reduction compared with control) and heart edema and this phenotype was confirmed using a second non-overlapping MO (Figure 3D and E). Interestingly, similar phenotypes are observed upon Shp2 knockdown in zebrafish [29]. Co-injection of a moderate

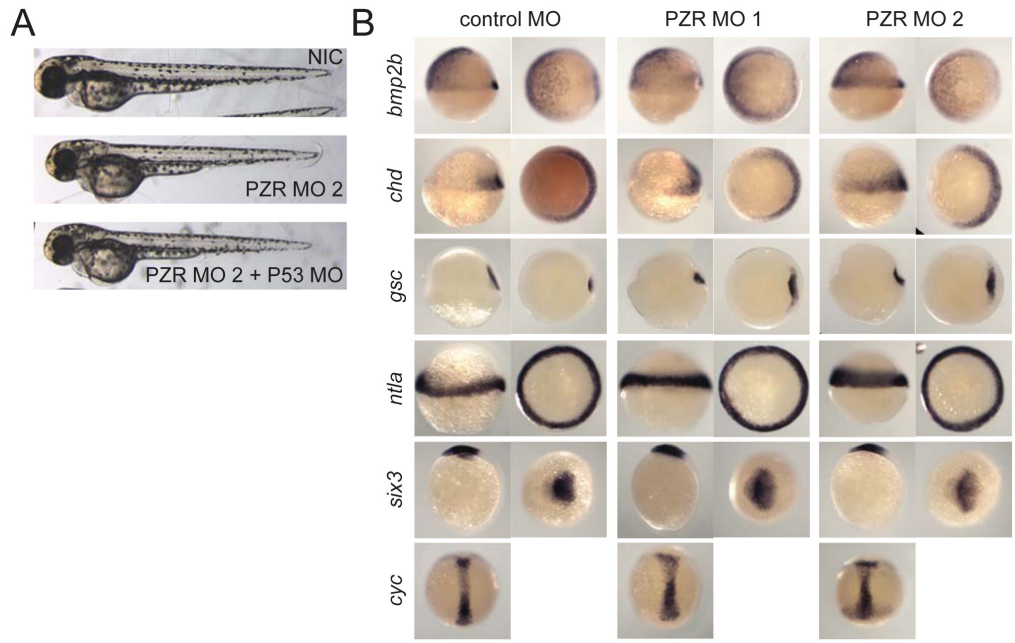

Figure 4. PZR knockdown is specific and does not affect cell specification (A) Zebrafish embryos were injected at the 1-cell stage with 2ng PZR MO alone or co-injected with p53 morpholino and photographed at 2 dpf. (B) Zebrafish embryos were injected at the 1-cell stage with 2 ng PZR MO1 or PZR MO2 or 2ng control morpholino, and fixed at shield stage (*bmp2b*, *chd*, *gsc*, *ntla*), 70% epiboly (*cyc*), and bud stage (*six3*) and probed for cell fate markers using *in situ* hybridization.

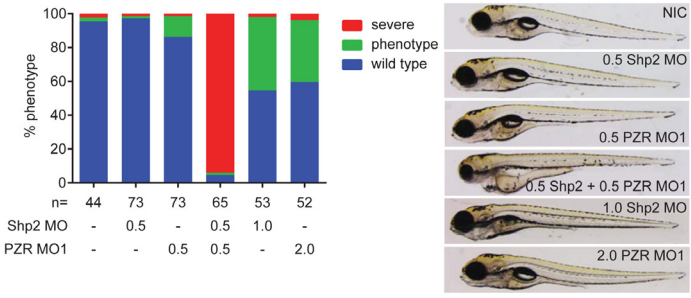

Figure 5. Genetic interaction between Shp2 and PZR. Embryos were injected at the 1-cell stage with Shp2 MO (0.5 pg) or PZR MO (0.5 pg), a combination thereof or Shp2 MO (1.0 pg) and PZR MO (2.0 pg). Embryos were imaged at 4 dpf. The stacked histogram in the left panel indicates quantitation of the phenotypes shown in representative photographs in the right panel.

dose of PZR mRNA (25 pg) rescued the PZR-MO-induced defects, whereas a higher dose of PZR mRNA (100 pg) failed to rescue (Figure 3D). To quantify the craniofacial defects in PZR knockdowns, embryos were fixed at 4 dpf and the cartilage was stained with alcian blue. The cartilage was greatly malformed and the angle of the ceratohyal displayed a significant increase, supporting the notion that PZR knockdown induced craniofacial defects, reminiscent of Shp2 knockdown [11] (Figure 3F).

The use of knockdown approaches by itself may lead to non-specific activation of p53 and subsequent apoptosis, thereby giving rise to developmental defects [30]. To rule-out this possibility we performed a co-knockdown of p53 and PZR, which did not attenuate the phenotype (Figure 4A). We subjected PZR knockdown embryos to *in situ* hybridization using a panel of cell

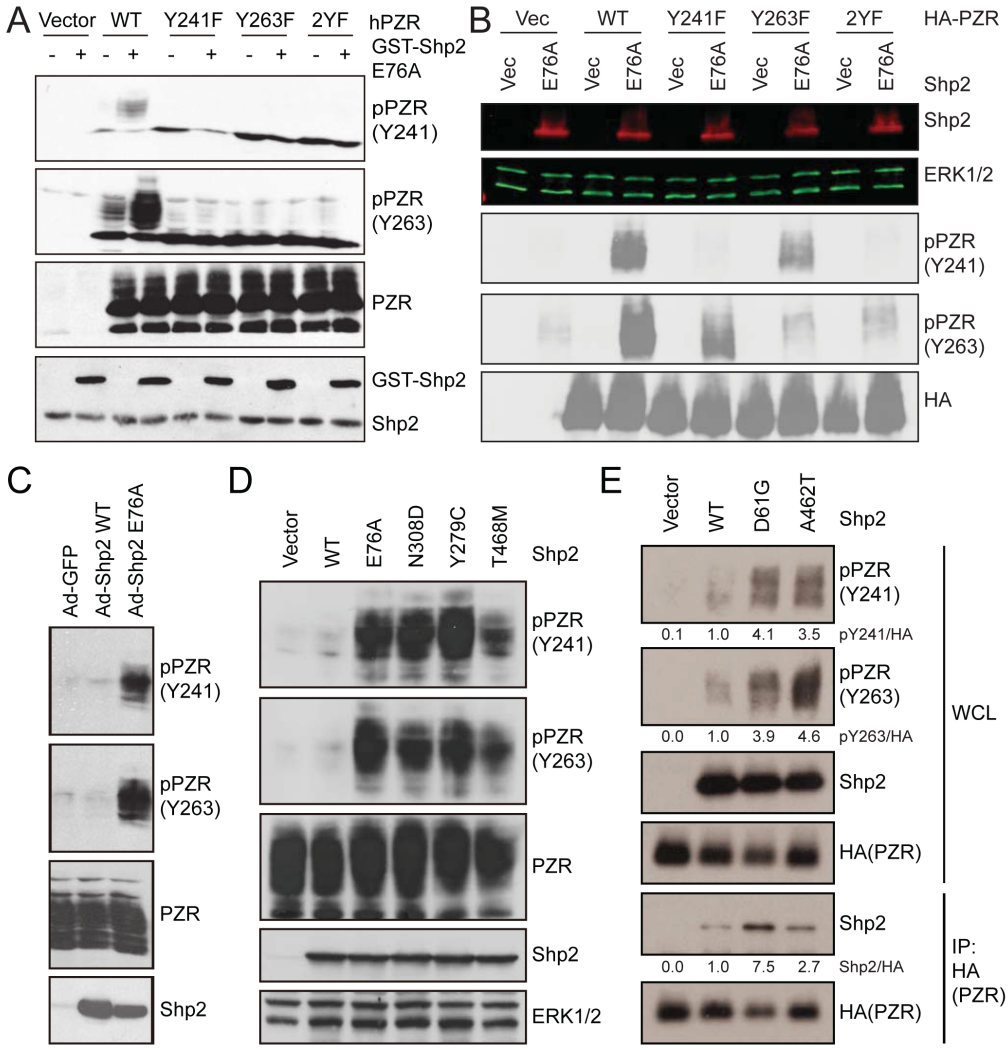

Figure 6. Characterization of PZR tyrosyl phosphorylation. (A) C2C12 cells were co-transfected with empty vector or activated GST-Shp2^{E76A} and either empty vector (vector), wild type human PZR (WT), PZR mutated at tyrosine 242 (Y241F), tyrosine 264 (Y263F), or both (2YF). Cell lysates were immunoblotted with anti-pPZR (Y241 or Y263), PZR or Shp2 antibodies. (B) HEK 293 cells were co-transfected with empty vector or activated Shp2E76A and either empty vector (vector), wild type zebrafish PZR (WT), PZR mutated at tyrosine 236 (Y241F), tyrosine 258 (Y263F), or both (2YF). Cell lysates were immunoblotted with anti-pPZR (Y241 or Y263), PZR or Shp2 antibodies. ERK1/2 was used as a loading control. (C) HUVEC cells were infected with adenoviruses expressing either GFP as a control, wild type Shp2 or Shp2E76A. Cell lysates were immunoblotted with anti-pPZR (Y241 or Y263), total PZR and Shp2 antibodies. (D) HEK 293 cells were transiently transfected with empty vector, wild type Shp2 (WT) or the indicated mutants of Shp2 (Activated Shp2; E76A, NS mutant; N308D or LS mutants; Y279C and T468M). Cell lysates were immunoblotted with anti-pPZR (Y241 or Y263), PZR and Shp2 antibodies. ERK1/2 was used as a loading control. (E) HEK 293T cells were transfected with HA-tagged zebrafish PZR with empty vector, wild type Shp2, Shp2D61G or Shp2A462T. Cell lysates were immunoprecipitated with anti-HA antibodies and immune complexes were immunoblotted with anti-Shp2 and anti-HA antibodies. Whole cell lysates were blotted with anti-pPZR (Y241 and Y263), Shp2 and HA

fate markers at shield stage (*gsc*, *bmp2b*, *chd, ntl*), 70% epiboly (*cyc*), and bud stage (*six3*). All markers were expressed indicating that cell specification was not affected (Figure 4B). Hence, PZR knockdown induced similar defects to those observed in both NS and LS Shp2 expressing embryos.

To investigate the genetic interaction between Shp2 and PZR, we partially knocked down Shp2 and PZR separately and together. If PZR is essential for Shp2 signaling, partial loss of both Shp2 and PZR should induce developmental defects that are more severe than by loss of each alone [29]. Knocking down Shp2 and PZR at sub-optimal levels did not induce developmental defects (Figure 5). However, partial knockdown of PZR and Shp2 together resulted in developmental defects at 4 dpf (Figure 5). The embryos were scored in three categories: wild type, phenotype and severe and it was evident that co-knockdown of Shp2 and PZR greatly enhanced the percentage of embryos displaying a severe phenotype (Figure 5). PZR knockdown also induced wider set eyes, reminiscent of the phenotype that we, and others, reported in Shp2 knockdowns [11,31]. Together, these results are consistent with the notion that PZR and Shp2 function in a conserved signaling pathway in zebrafish.

NS- and LS-associated Shp2 mutants induce PZR Y241 and Y263 hypertyrosyl phosphorylation.

We investigated the characteristics of PZR hypertyrosyl phosphorylation in further detail. To accomplish this, antibodies against tyrosyl phosphorylated PZR at Y241 (pY241-PZR) and Y263 (pY263-PZR) were generated. When cells were co-transfected with PZR, along with an activating mutant of Shp2 ($Shp2^{E76A}$) that induces PZR hypertyrosyl phosphorylation [25] both anti-pY241 and anti-pY263-PZR antibodies recognized tyrosyl phosphorylated PZR (Figure 6A). When Y263 in PZR was mutated to F263, neither anti-pY241 nor anti-pY263-PZR antibodies detected tyrosyl phosphorylated PZR upon co-expression of $Shp2^{E76A}$ (Figure 6A). Similarly, mutation of Y241 to F241 in PZR, also resulted in the failure of both anti-pY241 and anti-pY263-PZR antibodies to detect tyrosyl phosphorylated PZR (Figure 6A). The explanation for these results is that Y241 is required for Y263 phosphorylation, and conversely, Y263 for Y241 phosphorylation. Similar observations have been made by others [21,32]. Importantly, mutation of Y241 and Y263 to non-phosphorylatable residues abolished the immunoreactivity of both phospho-specific PZR antibodies (Figure 6A). These antibodies also recognized Y241 and Y263 in zebrafish PZR (Figure 6B).

We tested whether activating Shp2 mutants induced either Y241-PZR or Y263-PZR tyrosyl phosphorylation in other cell types. To this end, wild type and activating Shp2E76A mutants were introduced into human umbilical vein endothelial cells. These results indicated that pY241-PZR and pY263-PZR antibodies recognized endogenous tyrosyl phosphorylated PZR at Y241 and Y263, respectively (Figure 6C). The LS mutant from human and zebrafish when expressed in 293 cells were capable of inducing PZR hypertyrosyl phosphorylation at both Y241 and Y263 (Figure 6D and E). As reported previously [33], increased zebrafish PZR tyrosyl phosphorylation correlated with enhanced PZR/Shp2 binding (Figure 6E). Hence, both NS and LS mutants in human and zebrafish enhance PZR tyrosyl phosphorylation.

PZR hypertyrosyl phosphorylation in NS and LS mice.

We determined whether PZR was hypertyrosyl phosphorylated in NS mice. Hearts isolated from 8 week-old wild type and $Ptpn11^{D61G/+}$ mice showed a significant increase in pY263-PZR tyrosyl phosphorylation as compared with wild type controls (Figure 7A). In addition, PZR hypertyrosyl phosphorylation was observed in the cortex of $Ptpn11^{D61G/+}$ mice (Figure 7B), as well as in the

kidney, liver and spleen of these mice (Figure 8A-C). Given that in cultured cells LS induces PZR hypertyrosyl phosphorylation (Figure 6D and E), we tested whether PZR is hypertyrosyl phosphorylated using *Ptpn11*$^{Y279C/+}$ knock-in mutant mice, which represented a human LS mutant [34]. Hearts from *Ptpn11*$^{Y279C/+}$ mice were isolated and, although to a much lesser extent to *Ptpn11*$^{D61G/+}$ mice, PZR was hypertyrosyl phosphorylated on Y263 (Figure 7C). In addition, PZR was robustly hypertyrosyl phosphorylated in the cortex of *Ptpn11*$^{Y279C/+}$ mice (Figure 7D). In agreement with these data, we also observed that when zebrafish embryos were injected to express either the NS or LS mutants, PZR was also hyper tyrosyl phosphorylated at Y241 and Y263 (Figure 7E). No apparent differences were observed in the basal levels of Shp2, phosho-ERK1/2 or phospho-Akt between either NS or LS mice (Figure 9A-D). Collectively, these results show that both NS and LS mutants induce PZR hypertyrosyl phosphorylation within the ITIM Shp2 binding motif of PZR in mice and zebrafish.

NS and LS mutants induce PZR hypertyrosyl phosphorylation by enhancing Src/Shp2/PZR complex.

In order to investigate the mechanisms underlying how both NS and LS mutants induce PZR hypertyrosyl phosphorylation, we examined the dependency of NS and LS mutants to induce PZR hypertyrosyl phosphorylation through the SFKs. ITIMs serve as potent Src family kinase (SFK) substrates and SFKs phosphorylate ITIMs within PZR [35]. Pharmacological inhibition of the SFKs by SU6656 impaired both NS- and LS-induced PZR hypertyrosyl phosphorylation at pY241 and pY263 (Figure 10A). Similar results were also observed with the activated E76A mutant (Figure 10B).

Next, we determined the ability of the activating Shp2 mutant to induce PZR hypertyrosyl phosphorylation in fibroblasts lacking the expression of *Src*, *Fyn* and *Yes* (SYF cells). Here, we found that an activating Shp2 mutant failed to induce PZR hypertyrosyl phosphorylation at Y241 and Y263 (Figure 11A). Consistent with this, a kinase-dead mutant of c-Src blocked the ability of the activated Shp2 mutant to induce PZR hypertyrosyl phosphorylation at these sites (Figure 11B). Both human and zebrafish PZR served as c-Src substrates in vitro (Figure 11C and D) and co-expression of a constitutively activated mutant of c-Src promoted tyrosyl phosphorylation of zebrafish PZR in cells (Figure 11E). Hence, c-Src phosphorylates human and zebrafish PZR at the Shp2 binding sites demonstrating that the SFKs likely mediates PZR hypertyrosyl phosphorylation. It has been previously suggested that the "open" conformations of both NS and LS mutants exhibit properties that increase their propensity to interact with other signaling proteins. Based upon our observations that SFKs may play a role we tested whether the SFKs are NS and/or LS binding targets. To test this, c-Src was immunoprecipitated from cells expressing either wild type Shp2, NS or LS mutants and these immune complexes were immunoblotted to detect for the presence of Shp2. We found that in both NS and LS expressing cells that the amount of NS/LS-Shp2 present in c-Src complexes was significantly greater as compared with wild type Shp2 expressing cells (Figure 12A).

To determine whether Src is present in PZR complexes and whether this is enhanced by the "open" conformation of mutated Shp2 we immunoprecipitated Src and assessed the extent of PZR interactions. We found that when Src was immunoprecipitated, PZR and Shp2 were present in the complex (Figure 12B). However, Src failed to co-immunoprecipitate with the form of PZR that was mutated in both the ITIMs but still exhibited enhanced Shp2 binding to the "open" conformation Shp2 mutants (Figure 12B). Wild type PZR, as expected was found to exist in a complex with Shp2 and this was further enhanced when either the activating or LS Shp2-containing mutation was

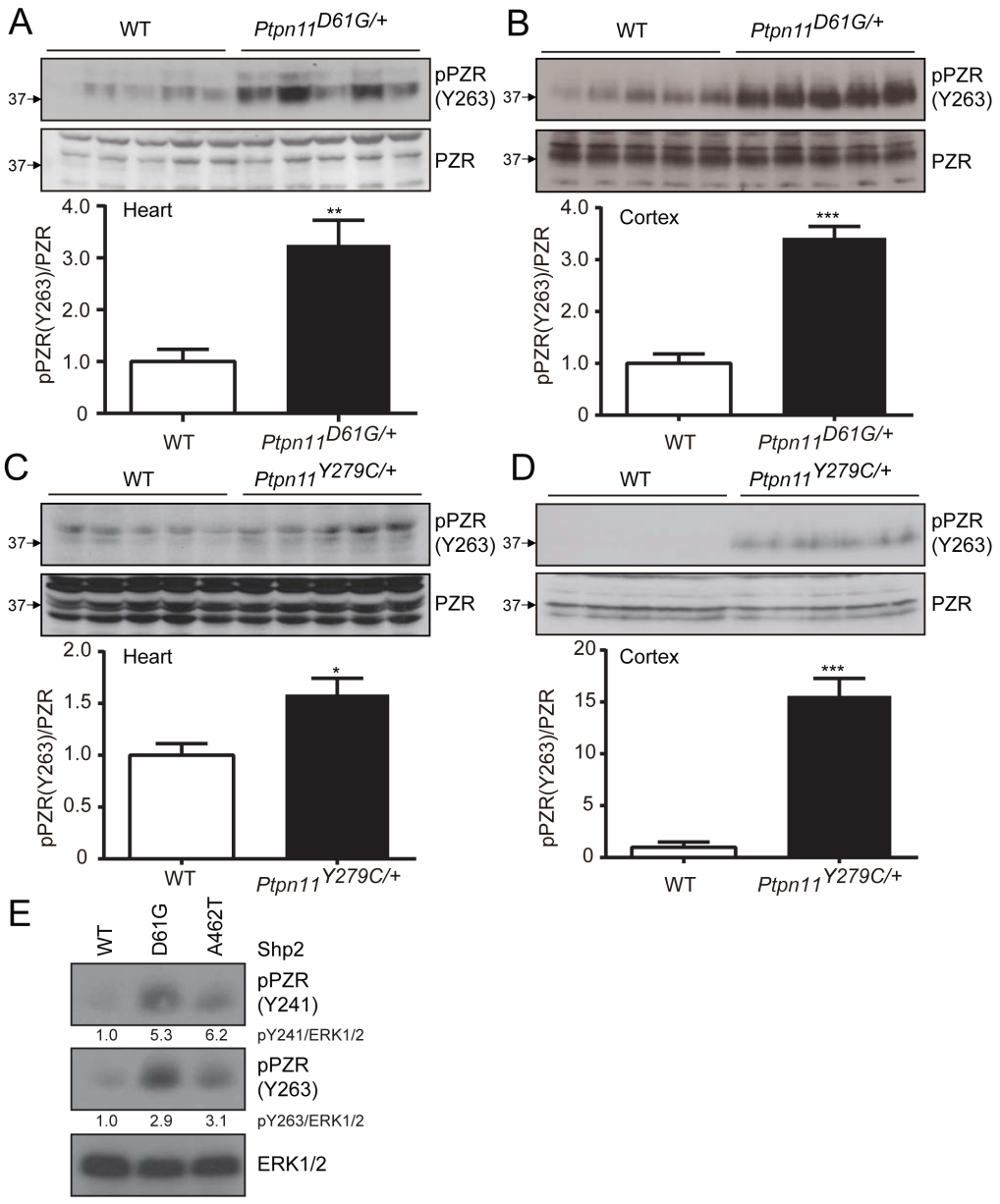

Figure 7. PZR tyrosyl phosphorylation in *Ptpn11*$^{D61G/+}$ and *Ptpn11*$^{Y279C/+}$mice and zebrafish expressing D61G or A462T Shp2. The heart (A and C) and the cortex (B and D) were isolated from 5-week-old WT and *Ptpn11*$^{D61G/+}$ mice (A and B) or 8-week-old WT and *Ptpn11*$^{Y279C/+}$ mice (C and D). Tissue lysates were immunoblotted with pPZR (Y263) and total PZR antibodies. Phosphorylation of tyrosine 264 in PZR represents n=5 per genotype. All data are mean ± S.E.M. *; P < 0.05, **; P < 0.01, ***; P < 0.001. (E) Lysates prepared from zebrafish embryos expressing either wild type, D61G or A462T Shp2 were immunoblotted with anti-PZR (pY241) and PZR pY263 antibodies. Relative quantitation shown below and ERK1/2 expression was used as a loading control.

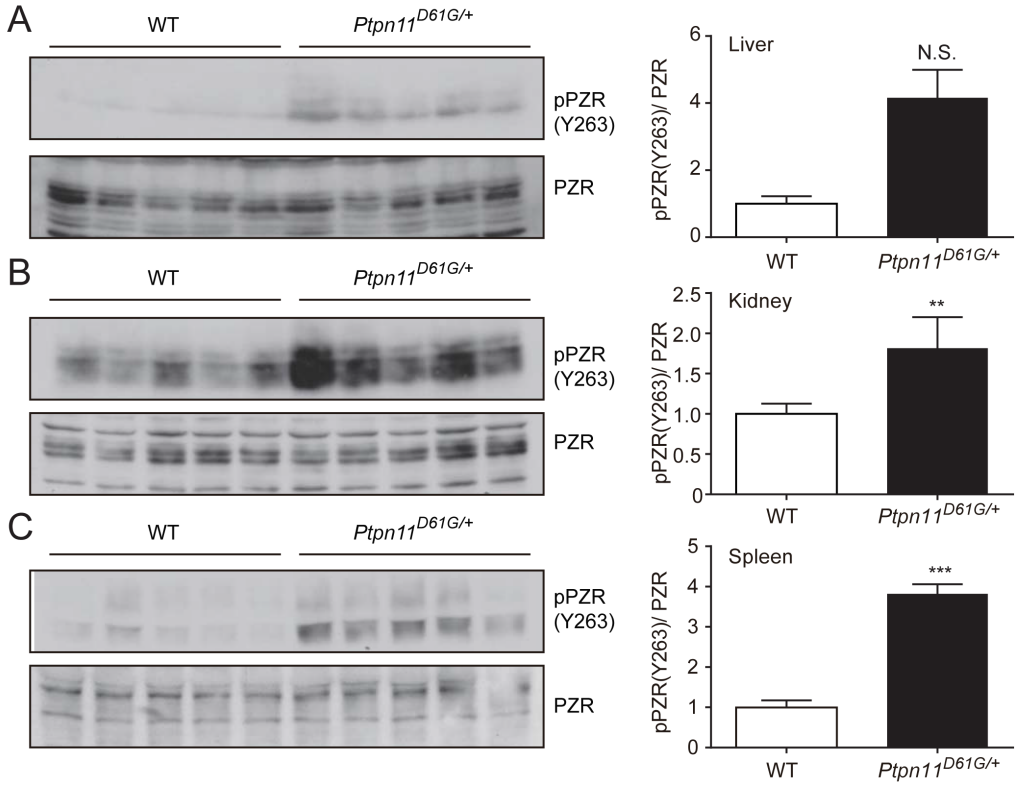

Figure 8 PZR tyrosyl phosphorylation in *Ptpn11*$^{D61G/+}$ mice. (A) liver, (B) kidney and (C) spleen were isolated from 5-week-old wild type and *Ptpn11*$^{D61G/+}$ mice. Tissue lysates were immunoblotted with anti-pPZR (Y263) and total PZR antibodies. Densitometric analysis of the phosphorylation levels of tyrosine 263 in PZR was determined and the results represent the mean ± S.E.M. from 5 mice per genotype. (**; P < 0.01, ***; P < 0.001; WT vs. NS).

expressed (Figure 12B). In contrast, double ITIM-containing mutant PZR, failed to form a complex (Figure 12B). These results suggest that the "open" conformation of Shp2 mutants exhibit an increased propensity to bind c-Src and that the likely explanation for PZR induced hypertyrosyl phosphorylation is causally related to the ability of Src to increase its proximity to PZR through Shp2 binding.

Convergence and extension defects induced by NS and LS are recapitulated by PZR in a phosphotyrosyl-dependent manner.

The similarities between the Shp2 [29] and PZR morphant phenotypes (Figure 3 and 5) indicate common defects during development. Previous results have shown that Shp2 knockdown and NS and LS *PTPN11* mutant overexpression lead to convergence and extension (C/E) cell movement defects during gastrulation resulting in shorter embryos with craniofacial defects and cardiac edema [11]. To test whether PZR knockdown also induces C/E defects, embryos were injected with PZR-, Shp2- or control morpholino, or LS mRNA as a positive control. Embryos were fixed at the 8- to 10-somite stage and subjected to *in situ* hybridization and stained for *krox20* and *myoD*, markers for rhombomeres three and five, and the somites, respectively. Loss of PZR led to shorter and wider embryos compared with controls at the same stage, and these phenotypes were similar

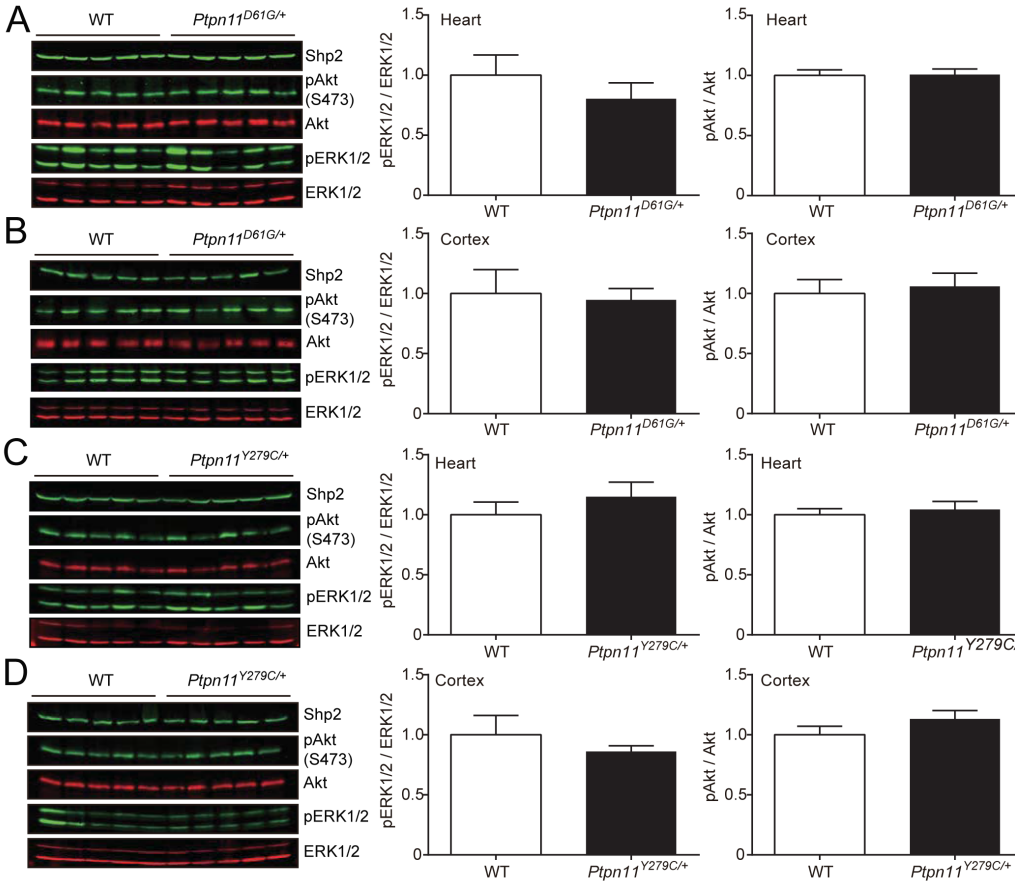

Figure 9. ERK and Akt phosphorylation in *Ptpn11*$^{D61G/+}$ and *Ptpn11*$^{Y279C/+}$ mice. The heart (A and C) and the cortex (B and D) were isolated from 5-week-old wild type and *Ptpn11*$^{D61G/+}$ mice (A and B) or 8-week-old wild type and *Ptpn11*$^{Y279C/+}$ mice (C and D). Tissue lysates were subjected to immunoblotting with anti-Shp2, pERK1/2, total ERK1/2, pAkt and Akt antibodies. Results represent densitometric analyses of the mean ± S.E.M. for pERK1/2 and pAkt from 5 mice per genotype.

to Shp2 knockdown and LS-Shp2 injected embryos (Figure 13A). These results indicated that PZR is essential for C/E cell movements, analogous to that of both NS and LS mutants during zebrafish gastrulation.

To assess whether PZR tyrosyl phosphorylation sites were important for C/E phenotypes we overexpressed wild type PZR and PZR tyrosyl phosphorylation site-deficient mutants and performed *in situ* hybridization at the 8- to 10-somite stage using markers for *krox20* and *myoD*. Overexpression of wild type PZR resulted in shorter and wider embryos (Figure 13B). When mRNA encoding double ITIM tyrosine to phenylalanine mutants (Y241F and Y263F; 2YF) and as a control mRNA encoding GFP were injected into zebrafish embryos the C/E phenotype was inhibited (Figure 13B). As expected, PZR tyrosyl phosphorylation and Shp2 binding to zebrafish PZR is inhibited in the double ITIM Y241F/Y263F mutant (Figure 13C). These data indicate that both tyrosyl phosphorylation sites within each of the ITIMs are required for PZR signaling for the promotion of the C/E phenotype during early development in zebrafish.

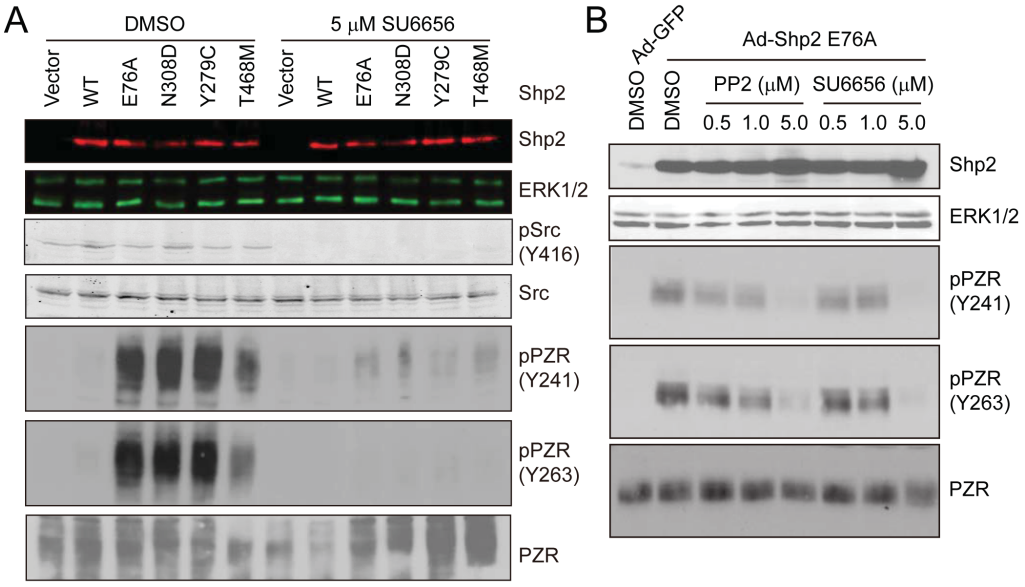

Figure 10. Effect of Src family kinases on PZR Y241 and Y263 phosphorylation. (A) HEK 293 cells were transiently transfected with the indicated Shp2 mutants and treated with either DMSO as a control or 5 μM SU6656. (B) NIH-3T3 cells were infected with the adenoviruses expressing either GFP as a control or a constitutively active Shp2E76A, in the presence of DMSO, PP2 or SU6656 at the indicated concentration. Cell lysates were immunoblotted with anti-Shp2, pSrc (Y416), Src, pPZR (Y241 or Y263) and total PZR antibodies. ERK1/2 was used as a loading control.

Discussion

Here, we identified using non-biased proteomic approaches PZR as a major hypertyrosyl phosphorylated protein in both NS and LS models of mice and zebrafish. Remarkably, disruption of PZR function resulted in similar phenotypes to that observed in NS or LS mutant expressing zebrafish. Mechanistically, NS and LS mutants induce PZR tyrosyl phosphorylation in a Src-dependent manner and these mutants acquire an enhanced Src interaction as compared with wild type Shp2. PZR is required for zebrafish gastrulation and tyrosyl phosphorylation is necessary to promote convergence and extension movements. Thus, NS and LS mutants function in a phosphatase-independent manner to promiscuously promote PZR hypertyrosyl phosphorylation leading to dysfunctional gastrulation. Collectively, these results suggest that PZR is a novel evolutionarily conserved target for NS and LS-associated Shp2 mutants.

The extracellular matrix serves to integrate dynamically processes that govern cell fate, tissue maintenance and homeostasis to outcomes that dictate organ architecture [36]. Growth factor receptors, chemokines and G-protein coupled receptors are either directly or indirectly influenced by the ECM to control cell proliferation, differentiation and cell survival. The "RASopathies" represent mutated components of the SOS/Ras/Raf/Erk and there has been much focus on the role this cascade plays in NS and LS as it relates to cell proliferation and cell survival [10]. PZR has been shown to function in the control of cell adhesion and migration [24,25,32,35,37]. Therefore, our findings imply that aberrant cell migration and adhesion likely play important roles in the pathogenesis of both NS and LS. The development of PZR mutant mice will be necessary to test these conclusions more comprehensively.

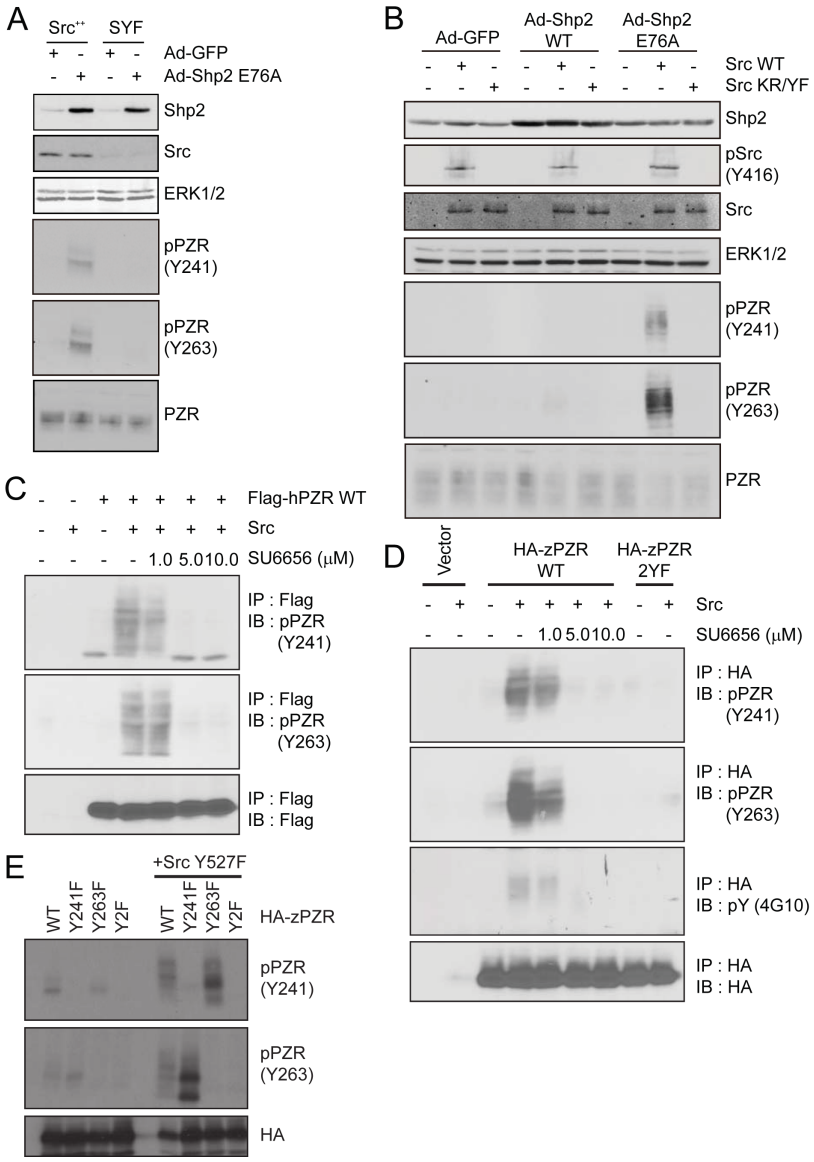

Figure 11. Src family kinases mediate NS/LS-induced PZR hypertyrosyl phosphorylation and increase NS/LS Src binding. (A) SYF (*Src*$^{-/-}$/*Fyn*$^{-/-}$/*Yes*$^{-/-}$ MEFs) and *Src*$^{+/+}$ (SYF-expressing wild type Src) cells were infected with adenoviruses expressing either GFP or Shp2 E76A. (B) SYF cells were transiently transfected with wild type c-Src or kinase-dead c-Src$^{K295R/Y527F\ (KR/YF)}$ and infected with adenoviruses expressing either GFP, wild type Shp2 or Shp2E76A. Cell lysates were immunoblotted with anti-Shp2, pSrc (Y416), pPZR (Y241 or Y263), PZR and Src antibodies. ERK1/2 was used as a loading control. (C and D) HEK-293 cells were transfected with Flag-tagged human PZR (C) or HA-tagged zebrafish PZR (D). The cell lysates were immunoprecipitated with indicated antibody. The immunoprecipitates were subjected to in vitro Src kinase assay with Src recombinant protein. The reaction products were immunoblotted with anti-pPZR (Y241 or Y263) antibodies. (E) HEK-293 cells were co-transfected with constitutively active Src mutant and either HA-tagged wild type zebrafish PZR (WT), PZR mutated at tyrosine 236 (Y241F), tyrosine 258 (Y263F), or both (2YF). Cell lysates were immunoblotted with anti-pPZR (Y241 or Y263) or HA antibodies.

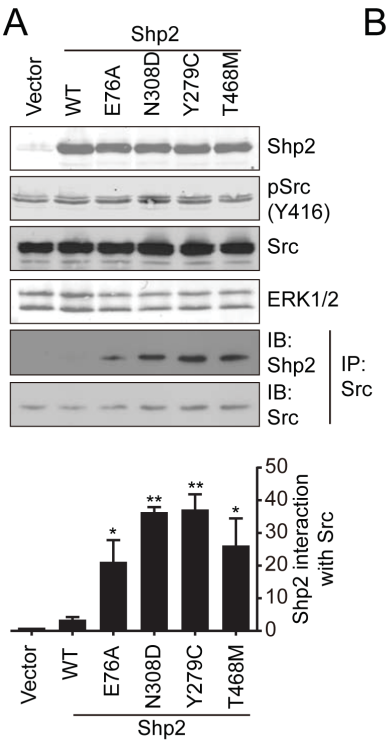

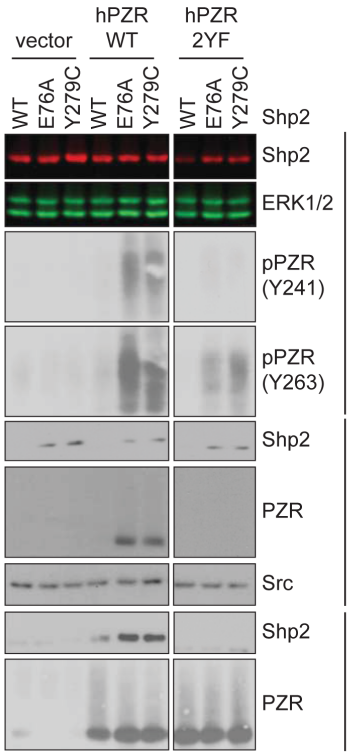

Figure 12. Enhanced Src complex formation with NS/LS-associated Shp2 mutants. (A) HEK 293 cells were transiently transfected either with Shp2 WT and the indicated Shp2 mutants. Cell lysates were immunoprecipitated with anti-c-Src antibodies and immune complexes immunoblotted with anti-Shp2 and anti-Src antibodies. The graph represents the mean ± SEM of the densitometric analysis from three independent experiments. Statistical significance is derived using a Dunnet's test comparing Shp2 mutants with WT. *, $P < 0.05$; **, $P < 0.01$. (B) HEK 293 cells were co-transfected with Shp2 WT, E76A or Y279C and either empty vector (vector), wild type human PZR WT or PZR 2YF mutant. Cell lysates were immunoblotted with anti-pPZR (Y241 or Y263) or Shp2 antibodies. ERK1/2 was used as a loading control. Immune complexes were immunoblotted with anti-Src, Shp2 and PZR antibodies.

Germline mutations in *Ptpn11* that result in either increased or decreased protein tyrosine phosphatase activity leads to developmental defects in zebrafish, mice and humans. Our findings that PZR is a target for *Ptpn11* mutations that exhibit either increased or decreased catalytic activity argue for a central role for PZR in ECM-mediated signaling for both NS and LS mutations. Using a zebrafish model system, we found that PZR is required for development. PZR RNA was apparent at early stages in zebrafish embryos, suggesting a maternal contribution and either knockdown or overexpression of PZR in zebrafish resulted in a gastrulation defect. PZR knock down in zebrafish resulted in similar defects to Shp2 and NS and LS-like phenotypes. In addition, partial knockdown of both PZR and Shp2 resulted in developmental defects. Together, this genetically links PZR to a pathway in which both NS and LS mutations participate. Importantly, we found that the loss of PZR in zebrafish led to convergence and extension defects, which is consistent with deterioration in the fidelity of cell migration. Intriguingly, overexpression of PZR induced gastrulation defects similar to that of both overexpression and reduced expression of Shp2, reported previously [11]. These results suggest a tight balance and interplay exist between PZR and Shp2 signaling, consistent with the biochemical evidence demonstrating that Shp2 binds directly to PZR within its ITIMs [11]. Collectively, these observations argue that PZR-mediated tyrosyl phosphorylation in zebrafish and mice serves as a mechanism to promote NS and LS signaling.

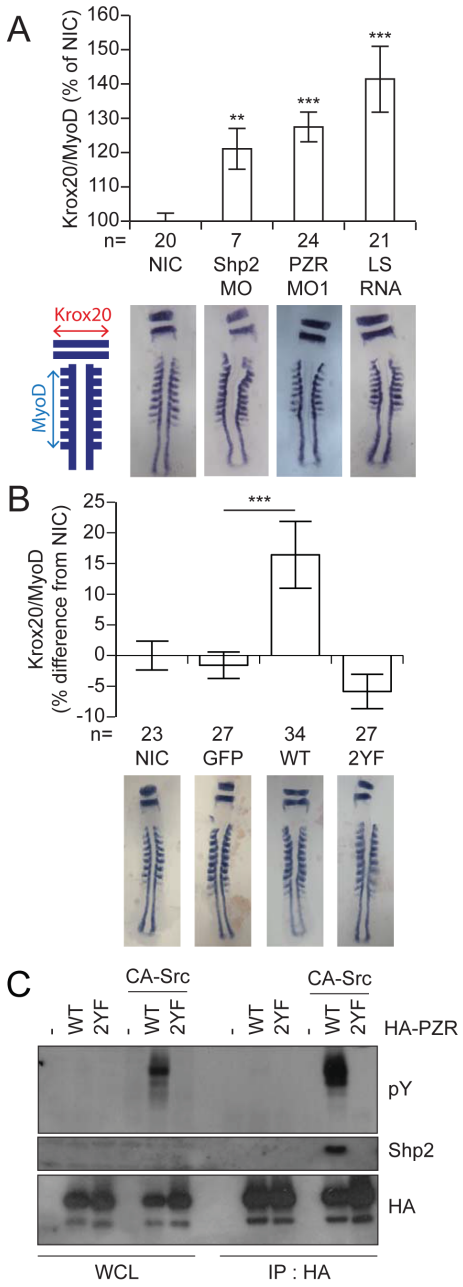

Figure 13. PZR tyrosyl phosphorylation is necessary for zebrafish convergence and extension phenotype. (A) Embryos were injected with Shp2 MO, PZR MO or LS mRNA at the 1-cell stage and fixed at the 8-10 somite stage. *In situ* hybridization was performed using *krox20* and *myoD* staining for rhombomeres 3 and 5, and somites, respectively. Quantification of the width of the rhombomeres (red) and the length of the first 8 somites (light blue) is shown schematically. *Krox20/myoD* ratios are plotted compared to non-injected controls (NIC). Data represent the mean ± S.E.M. **; P < 0.01, ***; P < 0.001. (B) Embryos were injected at the 1-cell stage with mRNA encoding GFP, wild type (WT) PZR or PZR with the indicated mutations. Ratios of *krox20/myoD* were calculated and compared to NIC. All data represent the mean ± S.E.M. ***; P < 0.001. (C) HEK-293 cells were co-transfected with either HA-tagged zebrafish PZR WT or 2YF mutant and constituvely active Src. Cell lysates were immunoprecipitated with HA antibody and blotted with anti-pY, Shp2 and HA antibodies.

What are the consequences of increased PZR tyrosyl phosphorylation? PZR acts as an adhesion-responsive glycoprotein where upon engagement to the extracellular matrix it becomes rapidly tyrosyl phosphorylated within its ITIMs. Upon tyrosyl phosphorylation Shp2 is recruited to PZR and it has been shown that this event is responsible for promoting the pro-migratory and cell adhesive effects in a variety of cell types [24,25,32,35,37]. Given the importance of cell migration and cell adhesion in developmental processes such as gastrulation it is conceivable that aberrant PZR tyrosyl phosphorylation induced by both NS and LS mutants disrupts this process. In mice, PZR is expressed during early development and we have demonstrated that PZR is hypertyrosyl phosphorylated in the developing embryo of *Ptpn11*$^{D61G/+}$ mice [25]. These observations support the notion that altered PZR tyrosyl phosphorylation and hence downstream signaling are associated with developmental defects. The significance of PZR tyrosyl phosphorylation was demonstrated in experiments in which overexpression of the ITIM mutants of PZR failed to induce gastrulation defects. These results define PZR tyrosyl phosphorylation as critical for development.

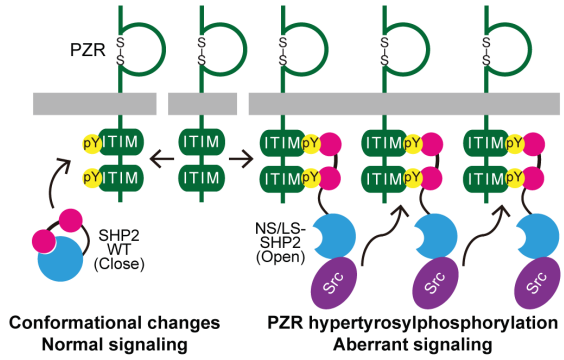

Figure 14. Model for the effects of NS and LS mutants on PZR tyrosyl phosphorylation. See text for details.

A provocative finding from our study is that these results implicate the actions of a tyrosine kinase that promotes PZR tyrosyl phosphorylation by both NS and LS mutants. The observation that PZR is hypertyrosyl phosphorylated in both NS and LS indicates that the ability of the kinase to phosphorylate PZR occurs in an Shp2 catalytically-independent manner. We had shown previously that enhanced PZR tyrosyl phosphorylation caused by NS mutants does not occur as a result of SH2 domain protection [25]. Rather, the data here supports a Src family kinase as responsible for NS and LS-induced PZR hypertyrosyl phosphorylation. Previous work had initially suggested a lack of SFK involvement in NS-mediated PZR hypertyrosyl phosphorylation [25]. In the Eminaga *et al.* study we immunoprecipitated Shp2 and analyzed total tyrosyl phosphorylation of Shp2-associated proteins. The Shp2-associated tyrosyl phosphorylated complex that migrated with a molecular weight of ~40kDa was found to contain at least PZR. It is likely that in this p40 complex that "site-specific" PZR tyrosyl phosphorylation was obscured by other co-migrating tyrosyl phosphorylated proteins. Whereas, in the experiments presented here, PZR tyrosyl phosphorylation is assessed directly using site-specific phospho-antibodies.

We found that both NS and LS mutants contain increased levels of c-Src complexes as compared with wild type Shp2. In addition, we showed increased PZR in Src complexes from activating and LS-associated Shp2 mutants and this was abolished in cells expressing the PZR tyrosyl phosphorylation-deficient mutant. The nature of this increased association with c-Src correlates with the common underlying property that both NS and LS mutants exhibit an "open" conformation [19,38]. Other groups have suggested that the "open" conformation of NS and LS may represent an important molecular mechanism for the pathogenesis of these mutant forms of Shp2 [19,20,31,38]. The open conformation of NS and LS mutants exposes the PTP and SH2 domains, presumably this presents binding surfaces for Src that are otherwise inaccessible. Indeed, it has been shown previously that Shp2 binds to Src through its SH3 domains [39,40]. Our findings support this observation, and extend it by providing a mechanism that reconciles the behavior of both NS and LS in their capacity to promote similar phenotypic outcomes.

The results from our proteomic screen are consistent with activation of a SFK-mediated pathway as we identified the Src substrate, focal adhesion kinase (FAK) and PECAM as hypertyrosyl phosphorylated in the hearts of NS mice. JNK was increased in its level of tyrosyl phosphorylation at one of its activating phosphorylation sites in NS hearts. Interestingly, Marin *et al.* showed that JNK and FAK were hypertyrosyl phosphorylated in LS mice suggesting a catalytic-independent mechanism for the activation of these molecules through the effects of enhanced Src function [34]. Whether or not PZR/Shp2/Src pathway accounts for the entirety of either NS or LS-like phenotypes will need to be determined. However, Jopling *et al.* have shown that Shp2 lies upstream of the SFKs in zebrafish development and the Shp2/SFK pathway is required for convergence and extension cell movements [11]. An integrated interpretation of our results support a model in which we invoke the actions of enhanced Src-mediated PZR tyrosyl

phosphorylation that results in altered development. An important aspect of Shp2-mediated signaling is that it is required to be appropriately localized to its upstream target. Disruption of the SH2 domains of Shp2 results in the abrogation of its ability to signal [1]. Therefore, enhanced PZR tyrosyl phosphorylation results in increased recruitment of Shp2 to PZR to promote further PZR tyrosyl phosphorylation and presumably other Src substrates that are in close proximity (Figure 14). It should also be noted that Src couples to Ras, and in some cases does so through Shp2 [41]. It is formally possible that both NS and LS engage Ras via this mechanism. However, the contribution of Ras signaling specifically for the manifestation of NS- or LS-related pathologies has yet to be determined. Collectively, these observations go some way towards providing an explanation as to how both the NS and LS mutants, which have enhanced and inactive PTP activities, respectively result in overlapping phenotypes.

In summary, we have identified PZR as a proximal target of both NS and LS mutants. PZR functions to regulate cell adhesion and cell migration. Therefore, in NS and LS the augmentation of PZR's interaction with Shp2 when it is hypertyrosyl phosphorylated presumably disrupts key developmental events that rely on the appropriate delivery of migratory ques. This mechanism occurs through enhanced binding of NS and LS mutants to Src. The implications of our findings clinically are that they suggest that the magnitude of PZR tyrosyl phosphorylation may reflect the "openness" of *Ptpn11* mutants and hence the severity of NS and LS-related diseases. As such, it would be instructive to assess the clinical genotype-phenotype relationship in context of PZR tyrosyl phosphorylation in NS and LS patients.

Materials and Methods

DNA constructs and cloning

Ptpn11 was cloned previously [11]. *Mpzl1* was cloned by nested PCR from zebrafish embryos (bud to 48hpf) cDNA with Phusion DNA polymerase (Finnzymes, Vantaa, Finland) using fwPZRout: 5'-GGGCGTTATTCATGAAATCTAAA-3', rvPZRout: 5'- CTCAGGTTGGCAGAGATGT-3', fwPZRstart: 5'- GCGGATCCATGGAAATAAGGCTT -3' and rvPZRstop: 5'-GCCGAATTCTCAGTTCTTGCGGATG-3'. PCR product was cloned into pCS2+ using BamHI and EcoRI. PZR ITIM mutants Y236F, Y258F and Y236F/Y258F were made using site-directed mutagenesis with the following primers:
Fw_Y>F236_PZR:5'-GGACCGGTGATTTTCGCTCAGCTCGAT-3'
Rv_Y>F236_PZR: 5'ATCGAGCTGAGCGAAAATCACCGGTCC-3'
RvstopY258F: 5'- CCGAATTCTCAGTTCTTGCGGATGTCTGCGAACACCACCGGCTC-3' PZR was then sub-cloned using BamHI and XhoI restriction enzymes into pSG5 vector encoding an RPTPa signal sequence and HA tag [42] using the following primers:
FwBamHI AGVSDPZR: 5'-GCCGGATCCGCCGGGGTCTCAGAT-3'
RvXhoI stopPZR: 5'-GCCCTCGAGTCAGTTCTTGCGGAT-3'.

Antibodies, chemicals, cell lines and expression reagents

Rabbit monoclonal phospho-PZR(Y241) and rabbit monoclonal phospho-PZR(Y263) antibodies were generated in collaboration with Cell Signaling. Mouse monoclonal Src antibody, rabbit polyclonal Src antibody, rabbit polyclonal phospho-ERK1/2(T202/Y204), mouse monoclonal ERK1/2 antibody, rabbit polyclonal phospho-Akt(S473) Ab and mouse monoclonal Akt antibodies were purchased from Cell Signaling. Rabbit polyclonal Shp2 antibodies and rabbit polyclonal ERK1/2 antibody were purchased from Santacruz Biotechnology. Mouse monoclonal Shp2 antibody was purchased from BD bioscience. Rabbit polyclonal PZR (105-6) was generously

provided by Dr. Z. J. Zhao. Src family kinase inhibitors, PP2 and SU6656, were purchased from Calbiochem. HEK-293, NIH-3T3, SYF (*Src*$^{-/-}$/*Yes*$^{-/-}$/*Fyn*$^{-/-}$ MEFs) and Src++ (Src overexpressing SYF) cells were purchased from ATCC and grown in growth medium (Dulbecco's modified Eagle's medium supplemented with 1% penicillin/streptomycin and 10% feral bovine serum) in a 5% CO2 incubator at 37°C. Replication-deficient adenoviral constructs harboring Shp2 WT (Ad-Shp2 WT), gain-of-function Shp2 mutant (Ad-Shp2 E76A) and GFP (Ad-GFP) were prepared as previously described [25,43]. NIH-3T3 and SYF cells were infected with by adenovirus at a dosage of 50 MOI. The pJ3 vectors containing Src WT and dominant negative Src mutant (Src K295R/Y527F) have been described in previously [44]. The pIRES-GFP plasmids encoding Shp2 WT, gain-of-function/Noonan syndrome mutants of Shp2 (Shp2 E76A and Shp2 N308D) and LEOPARD syndrome mutants of Shp2 (Shp2 Y279C and Shp2 T468M) have been described in previously [15,25]. DNA transfection into HEK-293 and SYF cells was performed using Lipofectamine 2000 according to the manufacturer's protocol. Mouse anti-phosphotyrosine antibody 4G10 (#05-321) from Merck Millipore, rabbit anti GFP (TP401) from Acris and mouse anti HA.11 clone 16B12 was from Covance.

Animal handling

Ptpn11$^{D61G/+}$ mice were provided from Dr. Benjamin Neel (University of Toronto, Toronto) and were genotyped as described previously [27]. Briefly, *Ptpn11*$^{D61G/+}$ male mice were crossed with WT C75BL/6 X SV129 female mice and their offspring were genotyped by PCR and digestion with AgeI for D61G allele. Animal handling was approved by The Yale University Institutional Animal Care and Use Committee. Tissues from *Ptpn11*$^{Y279C/+}$ mice were provided by Dr. Maria Kontaridis (Harvard University, MA).

In situ *hybridization*

Zebrafish were kept and embryos were staged as described (Westerfield 1995). *In situ* hybridizations were performed as described in Thisse *et al*., 1993. *Bmp2b*, *chd*, *gsc*, *ntla*, *dlx3*, *hgg, krox20* and *myod* probes were as described [11,45]. Antisense and sense *Mpzl1* probe was synthesized by T7 and SP6 mRNA polymerase (Promega), from pCS2+PZR, respectively.

Morpholino's RNA and injections – Zebrafish were kept and embryos were injected at the 1-cell stage. PZR morpholino 5'-CAGAGACCCTTACTGTGGTGGGACGC-3', Shp2 morpholino 5'-GGTGGAACCACCTTCGGGATGTCAT-3', nacre morpholino 5'-CATGTTCAACTATGTGTTAGCTTCA-3' and standard P53 morpholino were from Genetools (Philomath, OR). 5'- capped sense synthetic mRNA was synthesized with SP6 or T7 mRNA polymerase using mMessage mMachine kit from Ambion . The amount of RNA that was injected at the 1-cell stage was optimized for each synthetic RNA. Morpholino's were titrated down to give a specific phenotype without inducing increased apoptosis as co-injection of 1nmol p53 morpholino did not attenuate the phenotype. Likewise, mRNA was titrated down to either induce a phenotype or to rescue a morpholino induced phenotype.

Immunoprecipitation and immunoblotting

Cells were lysed on ice in lysis buffer (20 mM Tris-HCl, 150 mM NaCl, 1 mM CaCl2, 1 mM MgCl2, 1% Nonidet P-40, 1 mM Na3VO4, 10 mM NaF, 1 mM benzamidine, 1 mM PMSF, 1 μg/ml pepstatin A, 5 μg/ml aprotinin, and 5 μg/ml leupeptin. Tissues from Noonan (NS) and LEOPARD (LS) mice were lysed by homogenizing with lysis buffer. Cell or tissue lysates were incubated at 4 °C for 30 min and clarified by centrifugation at 14,000 rpm at 4 °C for 10 min. Protein concentration was determine using the BCA reagent according to the manufacturer's instructions (Pierce). For

immunoprecipitations, 500 μg of lysate was incubated with 1 μg of indicated antibodies at 4 °C for overnight. Immune complexes were collected on either protein A- or protein G-Sepharose beads for 4 hr at 4 °C, washed three times with same lysis buffer and then heated to 95 °C in sample buffer for 5 min. Total cell or tissue lysates and immune complexes were subjected to SDS-PAGE and immunoblotting. The sites of antibody binding were visualized using enhanced chemiluminescence detection or Odyssey Imaging System.

Transfected cells were lysed in RIPA buffer (150 mM NaCl, 20 mM Tris pH 8.0, 10 mM Na_2HPO_4, 5 mM EDTA, 1 mM Na-orthovanadate, 10% glycerol, 1% NP-40, 1% Sodium deoxycholate, 0,1% SDS, sodium fluoride 2.5 mM, β-glycerolphosphate 5 μM, aproptinin 1 μg/ml, leupeptin 1 μg/ml) for 15 minutes on ice with 1 ml per 10 cm dish. Samples were centrifuged for 30 min at 14,000 rpm 4°C. Then samples were pre-cleared using protein A agarose beads for 1 hr, an aliquot of whole cell lysate was immunoprecipitated with 1 μg antibody against HA for approximately 1hr on ice. Samples were precipitated using 25 μl protein A agarose slurry for approximately 1 hr at 4°C. Samples were boiled in 2x laemmli buffer and SDS-PAGE was performed.

For zebrafish, bud stage embryos were snap frozen in liquid nitrogen and stored in -80°C. Subsequently embryos were ground in cell lysis buffer containing 50 mM Tris, pH 7.5, 150 mM NaCl, 1 mM EDTA, 1 mM sodium orthovanadate, 1% Nonidet P-40, 0.1% sodium deoxycholate , sodium fluoride 2.5 mM, β-glycerolphosphate 5mM, aproptinin 1μg/ml, leupeptin 1μg/ml . Samples were then boiled in Laemmli sample buffer containing 4% SDS and β-mercaptoethanol. Proteins equivalent to 4 embryos per lane were subjected to SDS-PAGE and blotted onto a PVDF membrane. After blotting, membranes were stained using coomassie blue to verify equal loading. 293T cells were maintained in DMEM/F12 medium containing penicillin streptomycin and 10% and 7.5% FCS, resspetively. For serum starvation experiments non-essential amino acids were added. 293T and COS7 cells were passed twice a week at 1:20 and 1:7 before transfection. Transfection of zebrafish PZR was performed using polyethyleneimide (PEI) from Sigma with 20 μg DNA. After transfection overnight, medium was replaced with serum and harvested 40 hr after transfection.

Mass Spectrometric Analysis

The PhosphoScan method was performed as previously described [28,46-48]. Wild type and Shp2 mutant (Noonan Syndrome) mouse hearts were homogenized, sonicated, and centrifuged to remove cellular debris. Total protein for each tissue was normalized using the ProteinPlus Coomassie Reagent (Pierce), and proteins were reduced, alkylated, and digested overnight using trypsin (Worthington). Resulting peptides were separated from non-peptide material by solid-phase extraction with Sep-Pak Classic C18 cartridges (Waters). Lyophilized peptides were re-dissolved, and phosphopeptides were enriched by immunoaffinity purification using pY-100 phosphotyrosine antibody (#9411, Cell Signaling Technology). Peptides were eluted with 0.15% TFA and concentrated with C18 spin tips immediately prior to LC-MS analysis.

Duplicate injections of each sample were run to generate analytical replicates and increase the number of MS/MS identifications from each sample. Peptides were loaded directly onto a 10 cm x 75 μm PicoFrit capillary column packed with Magic C18 AQ reversed-phase resin. The column was developed with a 45-minute linear gradient of acetonitrile in 0.125% formic acid delivered at 280 nL/min. Tandem mass spectra were collected with an LTQ-Orbitrap XL mass spectrometer running XCalibur using a top 10 method, a dynamic exclusion repeat count of 1 and a repeat duration of 30 seconds. MS spectra were collected in the Orbitrap component of the mass

spectrometer, and MS/MS spectra were collected in the LTQ.
MS/MS spectra were processed using SEQUEST and the Core platform (Gygi Lab, Harvard University) [49-52]. Searches were performed against the mouse NCBI database with reverse decoy databases included for all searches to estimate false positive rates. Peptide assignments were obtained using a .98 precision cut-off in the linear discriminant analysis module of Core. Cysteine carboxamidomethylation was specified as a static modification, and methionine oxidation and serine, threonine, and tyrosine phosphorylation was allowed. Results were further narrowed using mass accuracy (–/+ 5ppm) filters and the presence of a phosphotyrosine in the peptide. Label-free quantitation was performed using Progenesis v4.1 (Nonlinear Dynamics). Peptide abundance data was manually reviewed in Progenesis for all peptides with at least a 2.0-fold change to ensure accuracy of results.

Global phosphotyrosine differential proteomic analysis in the heart

Heart tissue was lysed in urea buffer (20 mM Hepes, pH 8.0, 9 M Urea, 1 mM sodium vanadate, 2.5 mM sodium pyrophosphate, 1 mM β-glycerophosphate). The lysate was sonicated and clarified by centrifugation. Tissue lysate was reduced by DTT and alkylated with iodoacetamide. Samples were then diluted 4 times with 20 mM Hepes to reduce Urea concentration to 2M, and digested by trypsin overnight at room temperature with gentle shaking. Phosphotyrosine-containing peptides were isolated using immobilized phospho-tyrosine specific antibody PY100 (PhosphoScan Kit; Cell Signaling Technology). Following immuno-purification, phosphotyrosine-containing peptides were analyzed by LC-MS/MS as described previously [48].

Acknowledgements

This work was supported by NIH grant R01 GM099801 (A.M.B.) and in part, by a grant from the Research Council for Earth and Life Sciences (ALW 819.02.021) with financial aid from the Netherlands Organization for Scientific Research (NWO) (to J.d.H.).

References

1. Neel BG, Guo H, Pao L (2009) SH2 Domain-Containing Protein Tyrosine Phosphatases. In: Bradshaw RA, Dennis EA, editors. Handbook in Cell Signaling. 2 ed. San diego: Elsevier. pp. 707-728.
2. Hof P, Pluskey S, Dhe-Pagganon S, Eck MJ, Shoelson SE (1998) Crystal Structure of the Tyrosine Phosphatase SHP-2. Cell 92: 441-450.
3. Mohi MG, Williams IR, Dearolf CR, Chan G, Kutok JL, et al. (2005) Prognostic, therapeutic, and mechanistic implications of a mouse model of leukemia evoked by Shp2 (*PTPN11*) mutations. Cancer Cell 7: 179-191.
4. Tiganis T, Bennett AM (2007) Protein tyrosine phosphatase function: the substrate perspective. Biochem J 402: 1-15.
5. Saxton TM, Henkemeyer M, Gasca S, Shen R, Rossi DJ, et al. (1997) Abnormal mesoderm patterning in mouse embryos mutant for the SH2 tyrosine phosphatase Shp-2. EMBO J 16: 2352-2364.
6. Yang W, Klaman LD, Chen B, Araki T, Harada H, et al. (2006) A Shp2/SFK/Ras/Erk Signaling Pathway Controls Trophoblast Stem Cell Survival. Dev Cell 10: 1-11.
7. Perkins LA, Larsen I, Perrimon N (1992) corkscrew encodes a putative protein tyrosine phosphatase that functions to transduce the terminal signal from the receptor tyrosine kinase torso. Cell 70: 225-236.
8. Neel BG, Gu H, Pao L (2003) The 'Shp'ing news: SH2 domain-containing tyrosine phosphatases in cell signaling. Trends Biochem Sci 28: 284-293.
9. Tartaglia M, Mehler EL, Goldberg R, Zampino G, Brunner HG, et al. (2001) Mutations in *PTPN11*, encoding the protein tyrosine phosphatase SHP-2, cause Noonan syndrome. Nat Genet 29: 465-468.
10. Tartaglia M, Gelb BD (2005) Noonan syndrome and related disorders: genetics and pathogenesis. Annu Rev Genomics Hum Genet 6: 45-68.
11. Jopling C, van Geemen D, den Hertog J (2007) Shp2 knockdown and Noonan/LEOPARD mutant Shp2-induced gastrulation defects. PLoS Genet 3: e225.
12. Runtuwene V, van Eekelen M, Overvoorde J, Rehmann H, Yntema HG, et al. (2011) Noonan syndrome gain-of-function mutations in *NRAS* cause zebrafish gastrulation defects. Dis Model Mech 4: 393-399.
13. Tidyman WE, Rauen KA (2008) Noonan, Costello and cardio-facio-cutaneous syndromes: dysregulation of the Ras-MAPK pathway. Expert Rev Mol Med 10: e37.
14. Gelb BD, Tartaglia M (2011) RAS signaling pathway mutations and hypertrophic cardiomyopathy: getting into and out of the thick of it. J Clin Invest 121: 844-847.
15. Kontaridis MI, Swanson KD, David FS, Barford D, Neel BG (2006) PTPN11 (Shp2) mutations in LEOPARD syndrome have dominant negative, not activating, effects. J Biol Chem 281: 6785-6792.
16. Tartaglia M, Martinelli S, Stella L, Bocchinfuso G, Flex E, et al. (2005) Diversity and Functional Consequences of Germline and Somatic PTPN11 Mutations in Human Disease. Am J Hum Genet 78: 279-290.
17. Hanna N, Montagner A, Lee WH, Miteva M, Vidal M, et al. (2006) Reduced phosphatase activity of SHP-2 in LEOPARD syndrome: consequences for PI3K binding on Gab1. FEBS Lett 580: 2477-2482.
18. Gelb BD, Tartaglia M (2006) Noonan syndrome and related disorders: dysregulated RAS-mitogen activated protein kinase signal transduction. Hum Mol Genet 15 Spec No 2: R220-226.
19. Yu ZH, Xu J, Walls CD, Chen L, Zhang S, et al. (2013) Structural and mechanistic insights into LEOPARD syndrome-associated SHP2 mutations. J Biol Chem 288: 10472-10482.
20. Qiu W, Wang X, Romanov V, Hutchinson A, Lin A, et al. (2014) Structural insights into Noonan/LEOPARD syndrome-related mutants of protein-tyrosine phosphatase SHP2 (*PTPN11*). BMC Struct Biol 14: 10.
21. Zhao R, Zhao ZJ (2000) Dissecting the interaction of SHP-2 with PZR, an immunoglobulin family protein containing immunoreceptor tyrosine-based inhibitory motifs. J Biol Chem 275: 5453-5459.
22. Zhao R, Zhao ZJ (2003) Identification of a variant form of PZR lacking immunoreceptor tyrosine-based inhibitory motifs. Biochem Biophys Res Commun 303: 1028-1033.
23. Zhao ZJ, Zhao R (1998) Purification and cloning of PZR, a binding protein and putative physiological substrate of tyrosine phosphatase SHP-2. J Biol Chem 273: 29367-29372.
24. Roubelakis MG, Martin-Rendon E, Tsaknakis G, Stavropoulos A, Watt SM (2007) The murine ortholog of the SHP-2 binding molecule, PZR accelerates cell migration on fibronectin and is expressed in early embryo formation. J Cell Biochem: [Epub ahead of print].
25. Eminaga S, Bennett AM (2008) Noonan syndrome-associated SHP-2/*Ptpn11* mutants enhance SIRPalpha and PZR tyrosyl phosphorylation and promote adhesion-mediated ERK activation. J Biol Chem 283: 15328-15338.
26. Saxton TM, Pawson T (1999) Morphogenetic movements at gastrulation require the SH2 tyrosine phosphatase Shp2. Proc Natl Acad Sci U S A 96: 3790-3795.
27. Araki T, Mohi MG, Ismat FA, Bronson RT, Williams IR, et al. (2004) Mouse model of Noonan syndrome reveals cell type- and gene dosage-dependent effects of *Ptpn11* mutation. Nat Med 10: 849-857.
28. Rikova K, Guo A, Zeng Q, Possemato A, Yu J, et al. (2007) Global survey of phosphotyrosine signaling identifies oncogenic kinases in lung cancer. Cell 131: 1190-1203.
29. Jopling C, den Hertog J (2005) Fyn/Yes and non-canonical Wnt signalling converge on RhoA in vertebrate gastrulation cell movements. EMBO Rep 6: 426-431.
30. Robu ME, Larson JD, Nasevicius A, Beiraghi S, Brenner C, et al. (2007) p53 activation by knockdown technologies. PLoS Genet 3: e78.
31. Stewart RA, Sanda T, Widlund HR, Zhu S, Swanson KD, et al. (2010) Phosphatase-dependent and -independent

functions of Shp2 in neural crest cells underlie LEOPARD syndrome pathogenesis. Dev Cell 18: 750-762.
32. Zhao R, Guerrah A, Tang H, Zhao ZJ (2002) Cell surface glycoprotein PZR is a major mediator of concanavalin A-induced cell signaling. J Biol Chem 277: 7882-7888.
33. Eminaga S, Bennett AM (2008) Noonan syndrome-associated SHP-2/*PTPN11* mutants enhance SIRPalpha and PZR tyrosyl phosphorylation and promote adhesion-mediated Erk activation. J Biol Chem 283: 15328-15338.
34. Marin TM, Keith K, Davies B, Conner DA, Guha P, et al. (2011) Rapamycin reverses hypertrophic cardiomyopathy in a mouse model of LEOPARD syndrome-associated *PTPN11* mutation. J Clin Invest 121: 1026-1043.
35. Kusano K, Thomas TN, Fujiwara K (2008) Phosphorylation and localization of protein-zero related (PZR) in cultured endothelial cells. Endothelium 15: 127-136.
36. Wickstrom SA, Radovanac K, Fassler R (2011) Genetic analyses of integrin signaling. Cold Spring Harb Perspect Biol 3.
37. Zannettino AC, Roubelakis M, Welldon KJ, Jackson DE, Simmons PJ, et al. (2003) Novel mesenchymal and haematopoietic cell isoforms of the SHP-2 docking receptor, PZR: identification, molecular cloning and effects on cell migration. Biochem J 370: 537-549.
38. Bocchinfuso G, Stella L, Martinelli S, Flex E, Carta C, et al. (2007) Structural and functional effects of disease-causing amino acid substitutions affecting residues Ala72 and Glu76 of the protein tyrosine phosphatase SHP-2. Proteins 66: 963-974.
39. Walter AO, Peng ZY, Cartwright CA (1999) The Shp-2 tyrosine phosphatase activates the Src tyrosine kinase by a non-enzymatic mechanism. Oncogene 18: 1911-1920.
40. Peng Z-Y, Cartwright CA (1995) Regulation of the Src tyrosine kinase and Syp tyrosine phosphatase by their cellular association. Oncogene 11: 1955-1962.
41. Zhang SQ, Yang W, Kontaridis MI, Bivona TG, Wen G, et al. (2004) Shp2 regulates SRC family kinase activity and Ras/Erk activation by controlling Csk recruitment. Mol Cell 13: 341-355.
42. van der Wijk T, Blanchetot C, Overvoorde J, den Hertog J (2003) Redox-regulated rotational coupling of receptor protein-tyrosine phosphatase alpha dimers. J Biol Chem 278: 13968-13974.
43. Kontaridis MI, Eminaga S, Fornaro M, Zito CI, Sordella R, et al. (2004) SHP-2 positively regulates myogenesis by coupling to the Rho GTPase signaling pathway. Mol Cell Biol 24: 5340-5352.
44. Fornaro M, Burch PM, Yang W, Zhang L, Hamilton CE, et al. (2006) SHP-2 activates signaling of the nuclear factor of activated T cells to promote skeletal muscle growth. J Cell Biol 175: 87-97.
45. van Eekelen M, Runtuwene V, Overvoorde J, den Hertog J (2010) RPTPalpha and PTPepsilon signaling via Fyn/Yes and RhoA is essential for zebrafish convergence and extension cell movements during gastrulation. Dev Biol 340: 626-639.
46. Guo A, Villén J, Kornhauser J, Lee KA, Stokes MP, et al. (2008) Signaling networks assembled by oncogenic EGFR and c-Met. Proceedings of the National Academy of Sciences 105: 692-697.
47. Rush J, Moritz A, Lee KA, Guo A, Goss VL, et al. (2005) Immunoaffinity profiling of tyrosine phosphorylation in cancer cells. Nat Biotechnol 23: 94-101.
48. Stokes MP, Farnsworth CL, Moritz A, Silva JC, Jia X, et al. (2012) PTMScan direct: identification and quantification of peptides from critical signaling proteins by immunoaffinity enrichment coupled with LC-MS/MS. Mol Cell Proteomics 11: 187-201.
49. Beausoleil SA, Villen J, Gerber SA, Rush J, Gygi SP (2006) A probability-based approach for high-throughput protein phosphorylation analysis and site localization. Nat Biotechnol 24: 1285-1292.
50. Elias JE, Gygi SP (2007) Target-decoy search strategy for increased confidence in large-scale protein identifications by mass spectrometry. Nat Methods 4: 207-214.
51. Huttlin EL, Jedrychowski MP, Elias JE, Goswami T, Rad R, et al. (2010) A tissue-specific atlas of mouse protein phosphorylation and expression. Cell 143: 1174-1189.
52. Yates JR, 3rd, Eng JK, McCormack AL, Schieltz D (1995) Method to correlate tandem mass spectra of modified peptides to amino acid sequences in the protein database. Anal Chem 67: 1426-1436.